BJRS

BRAZILIAN JOURNAL
OF
RADIATION SCIENCES
11-04 (2023) | 01-17 | e2325

An easy and direct protocol based on planar molecular images to quantify ^{131}I using thyroid phantom

Apaza-Veliz[a,c], D.G.; Santos[a,b], V.F.; Franze[a], D.L.;

Matos-Alves[b],W.E.F.; Moraes[a*], E.R.

[a]*Departament of Physics-FFCLRP, University of São Paulo, Ribeirão Preto, Brazil*

[b]*Departament of Nuclear Medicine, Barretos Cancer Hospital, Barretos, Brazil*

[c]*Escuela Profesional de Física, Universidad Nacional de San Agustin de Arequipa, Arequipa, Peru*

**edermoraes@usp.br*

ABSTRACT

A planar nuclear medicine image can be used to estimate dosimetry during iodine therapy. To this end, radionuclide activity distribution should be quantified in the patient's body in terms of a calibration coefficient. This coefficient allows the net counts to correlate with the image's activity. This study aims propose a simple and easy calibration protocol to quantify ^{131}I activity in thyroid phantom by molecular planar images. Were acquired 13 planar images of different phantoms: thyroid phantom of symmetrical lobes; thyroid phantom of asymmetrical lobes; the Jacszack cylinder phantom with a syringe surrounded by air and water, and finally a plastic bottle containing a syringe with radionuclide. We applied the ^{131}I radionuclide in a General Electric gamma camera, model Discovery NM/CT 670 with a high energy general purpose parallel hole collimator above the phantoms positioned at camera bed. The calibration coefficient of the gamma camera and the standard deviation were determined for each phantom; the average calibration coefficient obtained was 0.062±0.006 MBq/cps. The results suggested that the phantoms applied as too the calibration coefficient obtained by them can provides reasonable value for the gamma camera calibration factor for iodine 131, therefore an accurate evaluation of the scattering media as the source detector distance could impose higher variability and uncertainties on results.

Keywords: **radionuclide imaging, nuclear medicine, radiologic phantom, thyroid gland, iodine therapy.**

ISSN: 2319-0612
DOI: https://doi.org/10.15392/2319-0612.2023.2325
Submitted: 2023-07-31
Accepted: 2023-11-21

1. INTRODUCTION

Molecular imaging is a diverse field, acquisition of static planar images is one of the main image modalities in nuclear medicine, regardless of the variations for diagnosis and treatment planning. The principle behind these images is based on the administration of a photon-emitting radionuclide along with pure or mixed substances with some specific drugs, which are structured and designed to move toward target tissues via biochemical pathways within the body [1, 2]. These substances are named radiopharmaceuticals, and they are used to collect images that show the physiological, biokinetic, and functional behavior of a targeted tissue or organ and provide molecular and cellular details in the human body or other living systems [2, 3]. Iodine 131 (^{131}I), which is administered to patients as sodium iodide (NaI), is a frequently employed radionuclide. It aids diagnosis and treatment of some thyroid disorders because the thyroid takes up iodine to produce the thyroid hormone [4-6]. ^{131}I emits gamma and beta minus radiation. Therefore, its gamma emission can be used to obtain images, while its beta minus emission enables molecular-level therapy [7]. Given that images are widely applied to evaluate and plan the treatment of thyroid illness, designing a simple and easily reproducible dosimetry protocol to quantify the radiation dose absorbed by patients treated with iodine is desirable.

In this scenario, we describe a simplistic, direct, and reproducible protocol based on ^{131}I and nuclear medicine planar images of five different phantom arrangements mimicking neck and thyroid to obtain a calibration factor that correlates the count in the nuclear medicine planar image to the real radionuclide activity inside the human body. The methodology follows the recommendations outlined in pamphlets 16 [8] and 24 [9] of the Committee on Medical Internal Radiation Dose-MIRD and has proven a good and reliable way to estimate the radiation dose that is delivered to the patient, thereby improving thyroid diagnosis and/or treatment planning and follow-up. The methodology allows radionucleotide activity to be quantified and the radiation dose received by a patient to be determined during acquisition of molecular image with ^{131}I during thyroid studies. This method can be further applied to other radionuclides or body regions.

2. MATERIALS AND METHODS

To obtain a calibration factor from the image counts of the ^{131}I uptake activity on the thyroid, 4 different phantoms modeling the neck with ^{131}I, on a sodium iodide solution, were used: two of these phantoms had different dispositions which led us to work in 5 different modelling scenarios and 13 measurements covering a variety of activity situations. The ^{131}I has radioactive half-life of 8.02 days, emits beta minus with mean kinetic energy of 606 keV in a ratio of 0.89 per decay, and a gamma photon of 364 keV in a ratio of 0.81 per decay. Anterior planar static images were acquired with a General Electric (GE) gamma camera, model Discovery NM/CT 670; a detection head with a parallel hole, high-energy, general-purpose collimator was employed.

2.1 Phantoms

The row of radioactive scattering medium modelling the thyroid and neck were: 1) a thyroid phantom of symmetrical lobes measuring 5.0 x 2.3 x 1.0 cm^3, with total phantom volume of 24 mL, involved by ten PolyMethyl MethAcrylate (PMMA) slabs measuring 20 x 20 x 1 cm^3 (Figure 1.a), in the following sequence from bottom to top, two slabs, the thyroid lobe, then eight slabs, named TS (Thyroid Symmetrical); 2) a neck simulator consisting of a cylinder with length of 12.5 cm and diameter of 12.5 cm, constructed with PMMA and a 3-cm cylindrical cavity where the spinal simulator structure was inserted and a thyroid symmetrical lobes measuring 5.9 x 2.9 x 1.0 cm^3 with a total volume of 28 mL (Figure 1.b), named NP (Neck Phantom); 3) a 3 liter plastic bottle (Figure 1.d), named PB (Plastic Bottle); and a cylindrical container of the Jaszczak phantom, BIODEX, model "Flangeless Deluxe ECT Phantom", 18,6 cm height and 20,4 cm diameter, with a volume of 6000 mL (Figure 1.c), these phantom were used in two ways, filled with water, named 4) JCw (Jaszczak with Water) and air 5) JCa (Jaszczak with air). The neck plus cervical spine and thyroid simulator was primarily built by Franzé, SPECT-CT images of the phantom were used as radioactive source (SPECT) and scattering media(CT) on ionizing radiation Monte Carlo simulation environment to estimate the radiation dose deposited into the imaged volume [10], on the basis of Cerqueira and Maia who evaluated two thyroid phantoms, one based on geometrically shaped, as the one we used, and another more anthropomorphically shaped, as options to mimetites normal and abnormal thyroids

functions, concluding that both can be used in nuclear medicine thyroid evaluations [11]. Then, the cervical spine simulator was modified for this study, to resemble reality more closely, since the reference had an aluminum cylinder as simulator. The original aluminum cylinder was replaced with seven small discs made of bone-equivalent material, with diameter of 3 cm and length of 1 cm, which simulated the vertebrae. The discs were intercalated with five other PMMA cylindrical discs, which also had diameter of 3 cm and length of 0.8 cm and simulated the intervertebral discs. A thyroid phantom of symmetric lobes was inserted in this modified neck phantom in a specific site at the neck simulator. For the most part, the use of cylindrical geometry simulators, including the plastic bottle, aimed to resemble the geometry of the neck as closely as possible in a simple and low-cost way, by using a quite common bottle of soda that can be found in any small store in Brazil. The iodine source into the JC phantom was in a 1 ml volume inside a 5 ml syringe and at plastic bottle on the edge of a 3 ml syringe into a microcentrifuge tube with a volume of 0.5 ml. The phantoms have a total volume as follow: the slabs 4L, neck phantom 1.8L. Deluxe cylinder 6 L and the Plastic Bottle 3L.

Figure 1: *Phantoms used to obtain images; a) symmetrical lobes thyroid phantom positioned between 2 and 8 PMMA slabs, b) neck phantom with thyroid symmetrical lobes and cervical spine, c) cylindrical Jacszack phantom filled with water (JCw) containing a syringe, and d) a plastic bottle with a syringe inside a microcentrifuge tube in syringe edge.*

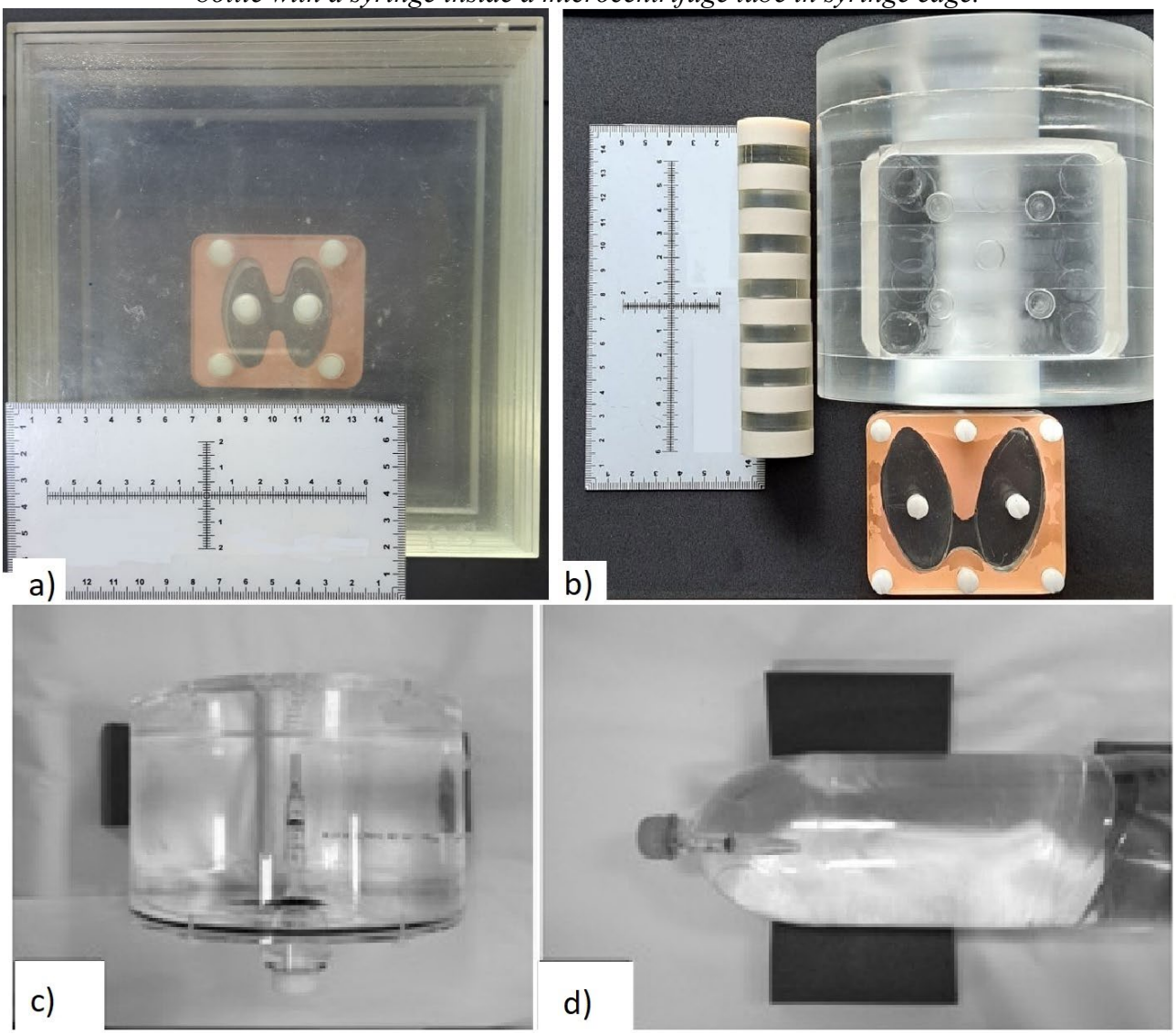

Source: Authors

2.2. ^{131}I activity measurement

The activities of ^{131}I homogenized in water, shown in Table 1, were obtained on an activimeter model CAPINTEC CRC-55tR. Since then, all the tests indicated in technical document 602 [12] and technical report 454 [13] have been conducted, and the equipment has been approved. The daily tests

indicated that the equipment provided reproducible results for a ^{133}Ba source with activity around 5.7 MBq, the average difference was -0.07%, the maximum difference was -0.1% with accuracy of -1.3%. According to the activimeter manual, ^{131}I was measured by accumulating counts for 4 and 25 seconds when the ^{131}I activity was above 0.74 MBq and below 0.74 MBq, respectively.

Each ^{131}I activity measurement was performed in triplicate with a minimal time interval of five seconds between them. The mean and twice the standard deviation value were used as the expected value for the ^{131}I activity and its uncertainty. Only statistic (type A) uncertainty was considered because uncertainties are far from well-established in the nuclear radioactive activity measurement type B. The syringe that was used in the cases when iodine was homogenized with water was washed with the solution and measured again in the activimeter. If the syringe presented any residual measurement, it was subtracted from the original measurement. In the case of the Jaszczak container and the plastic bottle, the syringe was directly positioned inside the phantom, as showed at figures 1c and 1d respectively.

2.3. Phantom Preparation and Acquisition Process

For practical reasons, the phantoms that were used for each image acquisition were named employing initial letters according to the phantom characteristic: a) TS for Thyroid Slabs, b) NP for Neck Phantom, c) JCa for cylindrical Jaszczak filled with air, d) JCw for cylindrical Jaszczak filled with water, and e) PB for Plastic Bottle. Table 1 lists the medium around or together with the radiopharmaceutical, the volume, the ^{131}I activity and its expanded uncertainties in a confidence level of 95%, or twice the standard deviation (SD), and the Source-Collimating Distance (SCD).

Table 1: *Different denominations for phantoms and their characteristics, as well as volume, ^{131}I activity, and distance for each acquisition.*

Denomination	Phantom	Volume (ml)	Activity ± 2SD (MBq)	SCD (cm)
TS	thyroid phantom of symmetric lobes + PMMA plates	22 (water)	39.48 ± 0.15 19.84 ± 0.19 9.92 ± 0.20 4.85 ± 0.15	5
NP	thyroid phantom of asymmetric lobes + neck + spine	27 (water)	42.23 ± 0.11 21.14 ± 0.15 10.72 ± 0.15 5.22 ± 0.15	
JCa	Cylinder + syringe containing radionuclide	6000 (air)	181.35 ± 0.11 109.18 ± 0.15	25
JCw		6000 (water)	181.35 ± 0.11 37.68 ± 0.11	
PB	Plastic Bottle	3000 (water + 10.98 ± 0.12 MBq)	129.53 ± 0.11	

In the case of the phantoms TS and NP, the symmetrical thyroid lobe was filled with 22 mL and 27 mL of water and ^{131}I activity, respectively. JC was filled with air or clean water, and ^{131}I was confined in 1 mL inside a 3-mL syringe, in the center of the circular cover. Likewise, a 3000-mL plastic bottle was filled with ^{131}I with activity of 3.67 ± 0.04 kBq/mL, homogenized in water. A 3-mL syringe with 1 mL of ^{131}I with activity of 129.52 ± 0.12 MBq was placed inside this bottle (Figure 1.d).

2.4. Image Acquisition and processing

The images were acquired at the Nuclear Medicine Department of the Barretos Cancer Hospital in a General Electric (GE) gamma camera model Discovery NM/CT 670; it used only one detection head with a parallel hole high-energy general-purpose collimator. The phantoms were positioned in the camera bed with the detector head number 01 above the phantom according to the source to distance informed at table1. The energy window was centered at 364 keV with a 20% acceptance energy range (327.6–400.4 keV), without zoom. The acquired images were stored in a 256 x 256 matrix with 1 x 1 mm^2 pixel size. Each image represented the accumulated counts over 360 seconds. Aiming for feasibility and reproducibility, a Region of Interest (ROI) based on contour lines was automatically generated. For the ROI edge, the contour line represented 30% of the maximum value

in the image. The total count inside the ROI represented the acquired counts, and twice the standard deviation of the counts corresponded to uncertainty.

2.5. Determination of the gamma camera calibration coefficient

To quantify the ^{131}I activity in the image, an imaging system calibration factor that is related to the information contained in the biodistribution images of the radiopharmaceutical had to be obtained. To this propose, the procedures indicated in the MIRD reports 16 [8] and 24 [9] were followed. The calibration factor for a gamma camera can be quantified by various methods such as single planar image [14,-15] conjugate image [16], and Monte Carlo simulation [17]. The calibration factor of the gamma camera (C_{cg}) is characteristic of each acquisition setup and represents the relationship between a known reference activity (A_r) and the net counts of a recognized region (r_f). The calibration factor can be determined by using the equation:

$$C_{cg} = \frac{A_r}{r_f} C_{cg} = \frac{A_r}{r_f} \quad (1)$$

C_{cg} has units of Mega becquerel (MBq) per counts per second (cps). To quantify the activity by a single plane image, a calibration factor that relates the activity directly to the net count rate of the organ or region of interest in the image is necessary:

$$A = C_{cg}.R_n A = C_{cg}.R_n \quad (2)$$

In equation 2, A is the activity in Mega becquerel (MBq), C_{cg} is the calibration factor ($MBq.cps^{-1}$) of the gamma camera, and R_n is the net count rate (cps).

2.6. Estimation of uncertainty and quantity comparison

In the cases where type A uncertainties such as the average C_{cg} value are reported, they were calculated by combining the calculation of the square of the uncertainty for the ^{131}I activity within two standard deviations in the pixel counts in the images considering a Poisson distribution, which

has a factor of coverage k = 2 according to the information presented in the system acquisition and image processing software; the aforementioned equations were employed. In general were used the expanded uncertainties in a confidence level of 95%, or twice the standard deviation (SD).Type B uncertainties have not been included due to inherent difficulties at the time of evaluation.

The Bland-Altman criterion [18] was used to compare the reference and measured activities values. This criterion allows comparisons to be made based on the correlation and agreement between the reference activity (A_{ref}) and the measured activity (A_{msd}) by using the calibration factor C_{cg} calculated for the gamma camera as a reverse check evaluation.

3. RESULTS AND DISCUSSION

Figure 2 (a-f) shows some representative images used to determine C_{cg} for different phantom types and activities: (a) TS; (b) NP; (c) JCw containing a syringe filled with 1 mL of ^{131}I with 181.3 MBq; (d) JCw with 109.2 MBq activity; (e) JCa containing a 181.3 MBq activity of ^{131}I into syringe; and (f) PB filled with 3000 mL of water, containing a syringe with 1 mL of ^{131}I with 129 MBq activity.

Figure 2: *Planar images of the phantoms for a) TS, b) NP, c) JCw with 181.3 MBq on a 1 mL syringe, d) JCw with 109.2.3 MBq on a 1 mL volume, e) JCa with 181.3 MBq on a 1 mL volume, and f) PB with 129MBq on a 0.5 mL volume.*

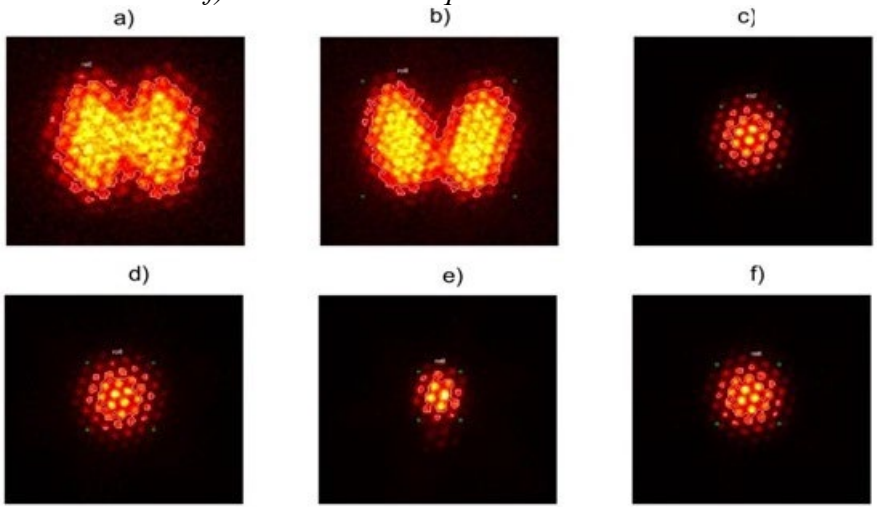

The table 2 contains the ^{131}I activity and the C_{cg} values obtained for each phantom configuration, the mean C_{cg} value $\bar{C}_{cg}$ and the percentage deviation among the $\bar{C}_{cg}$ with the associated uncertainties.

Table 2: *Presents the ^{131}I activity, the C_{cg} values obtained from the ^{131}I images, the mean $\bar{C}_{cg}$, and the percentage difference among C_{cg} and $\bar{C}_{cg}$ in each measurement. The uncertainties were calculated as the twice of the standard deviation, considering the standard deviation of each measurement, or on the assumption the data presents Poisson distribution in the image counts, excepted to $\delta\bar{C}_{cg}$ that is the uncertainty propagation from the original measurements. The percentage difference presents the values before the final rounding. The intermediary uncertainty was used with two algorisms since most of the then starts with 1 or 2.*

Phantom	**Activity ± 2SD (MBq)**	**C_{cg} ± 2SD (MBq/cps)**	$\bar{C}_{cg} \pm \delta\bar{C}_{cg}$ **(MBq.cps^{-1})**	**Percentage difference (%)** $(C_{cg} - \bar{C}_{cg})/\bar{C}_{cg}$
TS	39.48 ± 0.15	0.049 ± 0.007		-22%
	19.84 ± 0.19	0.051 ± 0.015		-18%
	9.92 ± 0.20	0.054 ± 0.028		-14%
	4.85 ± 0.15	0.054 ± 0.042		-14%
NP	42.23 ± 0.11	0.058 ± 0.007		-7%
	21.14 ± 0.15	0.056 ± 0.013		-10%
	10.72 ± 0.15	0.058 ± 0.022	0.062 ± 0.006	-7%
	5.22 ± 0.15	0.069 ± 0.040		10%
JCa	181.35 ± 0.11	0.076 ± 0.003		22%
	109.18 ± 0.15	0.078 ± 0.004		25%
JCw	181.35 ± 0.11	0.068 ± 0.003		9%
	37.68 ± 0.11	0.066 ± 0.007		6%
PB	129.53 ± 0.11	0.075 ± 0.003		20%

As shown in Table 2, the values obtained for each specific configuration and the average values obtained in the same configuration resembled each other, so the overall values presented a minimum value of 0.049 MBq.cps^{-1}, a maximum value of 0.078 MBq.cps^{-1}, and an average C_{cg} value of 0.062 MBq.cps^{-1} with a combined uncertainty of 0.006 MBq.cps^{-1}. The percentage difference between the $\mathbf{C_{cg}}$ values and its average range from -22% to 20%. Besides the phantom's dimensions varies significantly which can contribute to different scattering situations as volume partial effects, both not evaluated. In the same direction the neck phantom shows less variability among the different activities applied. Considering the lowest values for the TS and NP phantom were measured at smaller distances, 5 cm the scattering radiation in the surrounding medium did not strikes the scintillator in the same intensity as the JCa, JCw and PB which were measured at 25 cm. A similar situation can be

considered among the TS and NP, in the different way, since the source were at top for the NP phantom and at 8 cm deeper at TS.

In the image, we obtained A_{msd} by using equation (2) and the average value of C_{cg}. Table 3 summarizes the A_{ref} and the A_{msd} values in the images for each of the different phantoms and the percent relative difference (RD) between them.

***Table 3**: Comparison of the reference activity (A_{ref}) with the measured activity (A_{msd}) and the percent relative difference (RD) between them.*

Denominatio n	**A_{ref} (MBq)**	**A_{msd} (MBq)**	**RD (%)**
TS	39.48 ± 0.15	49.47 ± 0.18	25.3
	19.84 ± 0.19	24.30 ± 0.31	22.4
	9.92 ± 0.20	11.36 ± 0.52	14.6
	4.85 ± 0.15	5.52 ± 0.77	14.0
NP	42.23 ± 0.11	45.29 ± 0.15	7.3
	21.14 ± 0.15	23.26 ± 0.25	10.1
	10.72 ± 0.15	11.55 ± 0.40	7.8
	5.22 ± 0.15	4.69 ± 0.59	-10.1
JCa	181.35 ± 0.11	147.78 ± 0.10	-18.5
	109.17 ± 0.15	86.23 ± 0.11	-21.0
JCw	181.35 ± 0.11	166.23 ± 0.10	-8.3
	37.68 ± 0.11	35.16 ± 0.15	-6.7
PB	129.52 ± 0.11	107.54 ± 0.11	-17.0

The relative difference between the reference and measured activities ranged from -21.0% to 25.3%.

The relative differences between the measured and the reference activities of the phantoms TS and NP tended to have values below average, whereas the other configurations, JCa, JCw, and PB tended to have values above average (see Tables 2 and 3). This could be due to the partial volume

effect. The ^{131}I activity was much higher for the three latter phantoms and was confined in a small volume of 0.5 mL inside a syringe. On the other hand, the lowest ^{131}I activity was achieved with NP, which may have been a marginal value within the uncertainty range.

The reference and the measured activities were also compared based on their correlation and agreement by using the Bland Altman method as an evaluation and comparison criterion. Figure 3 shows the comparisons between the reference and the measured activities obtained from the images by using the Bland-Altman method.

In the situation that the phantoms resemble reality more closely, i.e., a small point source in the case of PB and JCw and intact thyroid in the case of NP, the C_{cg} values or the A_{meas} values were more similar despite being on different sides of the average, which is acceptable. This indicated that the C_{cg} value could be different for very small or broader sources mainly due to volume partial effect, which should be further evaluated in future works.

The Bland-Altman test, figure 3a, indicates strong linearity between the reference and the measured activities, with a correlation value r = 0.99, and 12 among the 13 acquisitions were inside a 95% confidence interval.

Figure 3: *Comparisons between the reference and the measured activities according the Bland-Altman test, a) the linear fit among measured and reference activity; b) the difference against the average activity (the average among reference and measured) with in an interval of twice de standard deviations(~95% confidence interval) following the Bland-Altman comparison test.*

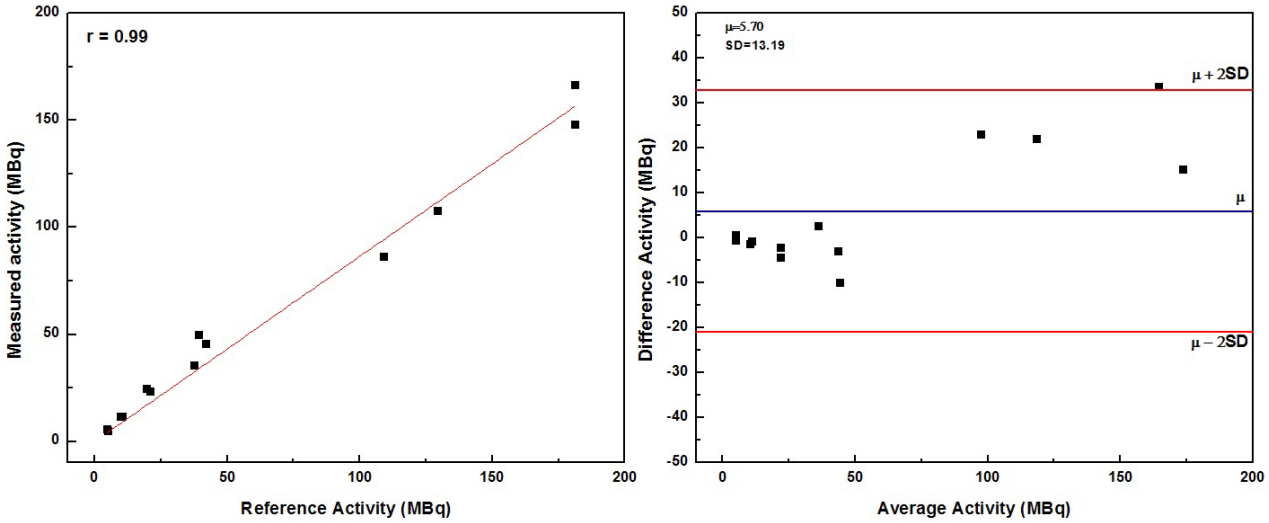

Summarizing the results demonstrate that an average gamma camera calibration coefficient can be easily obtained, thereby allowing radionuclide activity to be quantified in ^{131}I molecular images during thyroid imaging protocols based on anterior planar images. The method is relatively easy and direct to be performed. The average C_{cg} value obtained with the GE NM/CT 670 gamma camera and the applied acquisition parameters was 0.062±0.006 MBq.cps^{-1}. Analysis by the Bland-Altman method suggested that the measured activity quantified by employing the average C_{cg} value strongly correlates with the reference activity: r = 0.99, and agreement is better than 95%, indicating that the average C_{cg} value can be used to quantify activity in ^{131}I planar images by means of the thyroid acquisition protocol based on the gamma camera used in this work. All the different phantom configurations provide a good C_{cg} value for the gamma camera employed herein, which reveals that this is a simple model that could be the first clinical nuclear medicine tool to be applied to quantify ^{131}I activity in planar molecular images for individual treatment planning and dosimetry.

Further analysis should be done to determine which one of the low-cost proposed phantoms could better mimetics the most realistic option, which we suggest being the NP or PB, the first has a much more

similar situation, therefore the most elaborated, while the plastic bottle, the simplest and inexpensive one. The PB could provide better consideration among the scattered radiation from the patient body detected. Which we suggest as the origin of the higher value obtained for the PB against the NP.

4. CONCLUSIONS

Among the different sources plus scattering medium scenario evaluated aiming a simple way of mimetite a reminiscent thyroid post thyroidectomy the results suggest that the cylindrical plastic bottle with some adjustment could be an easy and good way to represent the conceived situation. Since it presented a closer geometric similarity with the more realistic one, the neck Phantom. Further experimental and simulation studies could better sustain the hypotheses, as indicate some adjustments into the plastic bottle modeling object to present a closer thyroid human situation, proportionating a simplest and cheapest way to gamma camera calibration factor to promote patient-specific thyroid treatment planning and follow-up.

ACKNOWLEDGMENT

We thank Departamento de Medicina Nuclear do Hospital do Câncer de Barretos for providing the gamma camera and the radiopharmaceutical. This study was partially supported by PRONABEC and Coordenação de Aperfeiçoamento de Pessoal de Nível Superior - Brasil (CAPES) - Finance Code 001; Conselho Nacional de Desenvolvimento Científico e Tecnológico (CNPq), and Núcleo de Apoio à Pesquisa em Física Médica, University of São Paulo, Ribeirão Preto, Brazil 2012.1.17619.1.0.

REFERENCES

[1] C. M. GOMES, A. J. ABRUNHOSA, P. RAMOS, AND E. K. J. PAUWELS, Molecular imaging with SPECT as a tool for drug development, **Adv. Drug Deliv. Rev**., vol. 63, no. 7, pp. 547–554, Jun. 2011, doi: 10.1016/j.addr.2010.09.015.

[2] D. A. MANKOFF, A definition of molecular imaging., **J. Nucl. Med**., vol. 48, no. 6, pp. 18N, 21N, Jun. 2007, [Online]. Available: http://www.ncbi.nlm.nih.gov/pubmed/17536102

[3] J. K. WILLMANN, N. VAN BRUGGEN, L. M. DINKELBORG, AND S. S. GAMBHIR,

Molecular imaging in drug development, **Nat. Rev. Drug Discov**., vol. 7, no. 7, pp. 591–607, Jul. 2008, doi: 10.1038/nrd2290.

[4] A. S. RILEY, G. A. G. MCKENZIE, V. GREEN, G. SCHETTINO, R. J. A. ENGLAND, AND J. GREENMAN, The effect of radioiodine treatment on the diseased thyroid gland, **Int. J. Radiat. Biol**., vol. 95, no. 12, pp. 1718–1727, Dec. 2019, doi: 10.1080/09553002.2019.1665206.

[5] F. XU, A. GU, Y. PAN, L. YANG, AND Y. MA, Analysis of iodine-131-induced early thyroid hormone variations in Graves' disease, **Nucl. Med. Commun**., vol. 37, no. 11, pp. 1154–1159, 2016, doi: 10.1097/MNM.0000000000000570.

[6] J. DER LIN, S. F. KUO, B. Y. HUANG, S. F. LIN, AND S. T. CHEN, The efficacy of radioactive iodine for the treatment of well-differentiated thyroid cancer with distant metastasis, **Nucl. Med. Commun**., vol. 39, no. 12, pp. 1091–1096, 2018, doi: 10.1097/MNM.0000000000000897.

[7] J. WEVRETT, A. FENWICK, J. SCUFFHAM, AND A. NISBET, Development of a calibration protocol for quantitative imaging for molecular radiotherapy dosimetry, **Radiat. Phys. Chem**., vol. 140, pp. 355–360, Nov. 2017, doi: 10.1016/j.radphyschem.2017.02.053.

[8] J. A. SIEGEL *et al.*, MIRD pamphlet no. 16: Techniques for quantitative radiopharmaceutical biodistribution data acquisition and analysis for use in human radiation dose estimates., **J. Nucl. Med**., vol. 40, no. 2, pp. 37S-61S, Feb. 1999.

[9] Y. K. DEWARAJA *et al.*, MIRD Pamphlet No. 24: Guidelines for Quantitative 131I SPECT in Dosimetry Applications, **J. Nucl. Med**., vol. 54, no. 12, pp. 2182–2188, Dec. 2013, doi: 10.2967/jnumed.113.122390.

[10] D. L. FRANZÉ, Dosimetria por imagem para o planejamento específico por paciente em iodoterapia, **Dissertação de Mestrado**, Universidade de São Paulo, 2016.

[11] R. A. D. CERQUEIRA AND A. F. MAIA, Development of thyroid anthropomorphic phantoms for use in nuclear medicine, **Radiat. Phys. Chem**., vol. 95, pp. 174–176, Feb. 2014, doi: 10.1016/j.radphyschem.2012.12.038.

[12] *Quality Control of Nuclear Medicine Instruments 1991*, no. 602. Vienna: INTERNATIONAL ATOMIC ENERGY AGENCY, 1991. [Online]. Available: https://www.iaea.org/publications/858/quality-control-of-nuclear-medicine-instruments-1991

[13] *Quality Assurance for Radioactivity Measurement in Nuclear Medicine*, no. 454. Vienna: INTERNATIONAL ATOMIC ENERGY AGENCY, 2006. [Online]. Available: https://www.iaea.org/publications/7480/quality-assurance-for-radioactivity-measurement-in-nuclear-medicine

[14] R. BARQUERO *et al.*, 131I activity quantification of gamma camera planar images, **Phys. Med. Biol**., vol. 62, no. 3, pp. 909–926, 2017, doi: 10.1088/1361-6560/62/3/909.

[15] R. BARQUERO et al, Procedimientos recomendados de dosimetría de pacientes en tratamientos de hipertiroidismo con I-131. Grupo de trabajo de dosis tras la administración de radiofármacos de la Sociedad Española de Física Médica. **Revista De Física Médica**, 18(2) pp. 143–176, 2017

[16] H. HÄNSCHEID *et al.*, EANM Dosimetry Committee Series on Standard Operational Procedures for Pre-Therapeutic Dosimetry II. Dosimetry prior to radioiodine therapy of benign thyroid diseases, **Eur. J. Nucl. Med. Mol. Imaging**, vol. 40, no. 7, pp. 1126–1134, Jul. 2013, doi: 10.1007/s00259-013-2387-x.

[17] Y. K. DEWARAJA, M. LJUNGBERG, AND K. F. KORAL, Characterization of scatter and penetration using Monte Carlo simulation in 131I imaging., **J. Nucl. Med**., vol. 41, no. 1, pp. 123–30, Jan. 2000,

[18] J. M. BLAND AND D. G. ALTMAN, Statistical methods for assessing agreement between two methods of clinical measurement., **Lancet** *(London, England)*, vol. 1, no. 8476, pp. 307–10, Feb. 1986